Inorganica Chimica Acta 502 (2020) 119317

Contents lists available at ScienceDirect

Inorganica Chimica Acta

journal homepage: www.elsevier.com/locate/ica

Research paper

Superprotonic conductivity of Ti-based MOFs with Brønsted acid–base pairs

Wei-Hua Deng[a,b], P. Naresh Kumar[a], Wen-Hua Li[a,b], Chiranjeevulu Kashi[a], Ming-Shui Yao[a], Guo-Dong Wu[a], Gang Xu[a,b,*]

[a] State Key Laboratory of Structural Chemistry, Fujian Institute of Research on the Structure of Matter, Chinese Academy of Sciences, Fuzhou, Fujian 350002, China
[b] University of Chinese Academy of Sciences, Chinese Academy of Sciences, Beijing 100049, China

ARTICLE INFO

Keywords:
Ti-based MOFs
Highproton conductivity
Brønsted acid–base pairs

ABSTRACT

Fuel cells technology demands high and stable proton-conductivity electrolyte materials. Here we show an effective approach of H_2SO_4 impregnation into Ti-based metal–organic framework (Ti-MOFs, $(NH_2)_x$-MIL-125 (x = 0, 1 or 2)), attains high proton-conductivity. The proton conductivity increases for increased amino functional groups on H_2SO_4@$(NH_2)_x$-MIL-125 (x = 0,1 or 2). The superproton conductivity, attributed to the abundant dangled amino functional groups, through an enhanced Brønsted acid–base pairs with sulfonic acid. Notably, the H_2SO_4@$(NH_2)_2$-MIL-125 measured to be superprotonic conductivity of 2.2×10^{-2} S cm^{-1} under 98% RH &80 °C, thus competes with the most popular electrolyte, such as Nafion. In addition, the composite appeals required characteristics of easy operation, and good stability.

1. Introduction

Developing renewable/clean energy sources to replace the fossil fuels, attracts considerable attention for the increased global clean-energy demand. Thus advances the energy storage/conversion technology to figure out the energy relevant issues. Proton exchange membrane fuel cell (PEMFC) is one of the promising technology owing to the low-pollutant emission, high-energy density and mild operating conditions [1–2]. High proton-conducting electrolyte materials offer multiple advantages to make hydrogen fuel cells more efficient. At present, most of the proton conductors are based on Nafion [3], organic polymers and inorganic solid acids [4]. However, most of them are non-crystalline structures, therefore difficult to exactly analysis the structure–activity relationship, and what is more, there is a challenging to well-defined control over the high-order structures. Synthetic well-established channel and crystalline structure materials are highly desired for proton conductor [5–6].

Metal-organic frameworks (MOFs), composed of metal ions or clusters bridged together with organic ligands, are well-known for its diversity of applications involves tunable-porosity, functionality, and crystallinity [7–30]. Of which, crystallinity can be coupled with many aspects of molecular-level designs, structural optimization and transport mechanisms [6]. Meanwhile, the tunable porosity and pore-dimensions can prevent unwanted fuel crossover in a PEMFC through filling pores with water and/or proton carrier [1,31–33]. Hallmark properties of MOFs make it suitable candidate for the development of proton conductors, such as the pioneering works of H. Kitagawa [2,4,33–39]. MOFs, as proton conductors, can be divided into water-assisted and water-repellent categories [2,40]. Alternatively, water-assisted proton-conducting MOFs have distinct characteristic of high performance at lower operation temperatures (20 to 80 °C) obeying the H-bond interactions with water molecules [41–42]. In general, the proton conductivity is dominated by the amount and mobility of H^+ ions [41]. So impregnating with low volatile acids, such as H_2SO_4 or H_3PO_4 into the MOF can amplify proton donors, thereby promotes the proton conductivity through the H-bond networks [1,37,43–44]. The relatively weak interactions of acid groups and MOF framework lead to high proton migration, but these acid groups are easy to get rid of the framework during the work conditions,which results in long-term stability issues. [45] For a proton conductor, both attaining high conductivity and maintain stability at the same time is very difficult through simplified approaches. Compounds with Brønsted basic sites (such as amines) and Brønsted acid sites (such as sulfonic acid) are tentative to fall into Brønsted acid–base pairs [2,42]. Brønsted acid–-base pairs play the key role achieving high and long-term proton conductivity for MOFs [4,44–45]. Thus, we succeeded in rational design of high and stabile proton conductive materials by introducing acid groups into amino functional MOFs with a facile way.

In this work, chemically stable Ti-MOFs, $(NH_2)_x$-MIL-125 (x = 0, 1 or 2) were directly synthesized by a modified one-pot method,[46] and

* Corresponding author at: State Key Laboratory of Structural Chemistry, Fujian Institute of Research on the Structure of Matter, Chinese Academy of Sciences, Fuzhou, Fujian 350002, China.
E-mail address: gxu@fjirsm.ac.cn (G. Xu).

https://doi.org/10.1016/j.ica.2019.119317
Received 4 August 2019; Received in revised form 4 November 2019; Accepted 27 November 2019
Available online 09 December 2019
0020-1693/

high proton-conducting complexes, H_2SO_4@$(NH_2)_x$-MIL-125 (x = 0, 1 or 2) were successfully developed by a facile impregnation way. The unique Brønsted acid–base pairs formed between H_2SO_4 and amino groups of MOF linkers build high-density H-bonding networks. We propose that the abundant dangling amino functional motifs have moderate interaction with sulfonic acid groups by the formation of Brønsted acid–base pair units, which resulted high proton conductivity and stability under humidified conditions. The proton conductivity increased with the increased amino functional groups of H_2SO_4@$(NH_2)_x$-MIL-125 (x = 0, 1 or 2). Among them, the H_2SO_4@$(NH_2)_2$-MIL-125 exhibited the highest super-proton conductivity of 10^{-2} S cm^{-1} at 98% RH and 80℃, competes with the most of the existed proton conductive MOFs under similar conditions.

2. Experimental details

2.1. Materials

All the chemicals and solvents used during MOF and modified MOF synthesis are commercially available and used them without further purification. Terephthalic acid (bdc), 2-Aminoterephthalate (bdc-NH_2) and 2, 5-diamino terephthalic acid (bdc-$(NH_2)_2$) were purchased from Alfa Aesar Co., China. Titanium *n*-butoxide ($Ti(OC_4H_9)_4$) and other solvents waere procured from Shanghai Chemical Reagent Co., China.

2.2. Preparation of H_2SO_4@$(NH_2)_x$-MIL-125 (x = 0, 1 and 2)

In order to obtain NH_2-MIL-125, bdc-NH_2 (2.172 g, 12 mmol) and titanium *n*-butoxide (0.208 mL, 0.6 mmol) were added in to a mixed solution containing dry DMF (18 mL) and dry MeOH (2 mL) taken in a 50 mL beaker. The above mixture was stirred at room temperature for 30 min and aliquot of 10 mL was transferred into a 20 mL teflon vessel placed in a stainless steel autoclave and heated at 150 °C for 72 h. After reaction, yellow powder of NH_2-MIL-125 nanosheets was obtained and washed with DMF and methanol consequently, and dried at 150 °C for 12 h. MIL-125 and $(NH_2)_2$-MIL-125 were prepared using the same protocol using the same amount of bdc ligand and bdc-NH_2/bdc-$(NH_2)_2$ ligand (molar ratio, 9/1), respectively.

The freshly made $(NH_2)_x$-MIL-125 (x = 0,1 or 2) samples were immersed into a 1 M of H_2SO_4 aqueous solution for three times with a time period of 5 min, and the obtained solid powders were collected and thoroughly washed with methanol in order to remove the residual H_2SO_4 and dried at 80 °C. The corresponding products were labeled as H_2SO_4@$(NH_2)_x$-MIL-125 (x = 0, 1 or 2) and used to the further characterizations.

2.3. Characterization

The morphology and structure were observed by SEM (JEOL JSM-6700F) and TEM (Tecnai F20). Powder X-ray diffraction (PXRD) was performed on a Rigaku Miniflex 600 powder diffractometer using Cu-Kα radiation (λ = 1.5418 Å), with 1°/min and 0.02° scan width between 5 and 40° 2θ. UV–vis spectrum was performed on a Perkin–Elmer Lambda 950. Infrared spectrums were obtained using MOF-KBr pellets on a VERTEX70 FT-IR spectrometer. Thermogravimetric analyses were carried out at a heating ramp of 10 °C/min in a N_2 flow (50 mL/min) using a STA449 instrument. Gas sorption isotherms were measured using a ASAP 2460 gas adsorption instrument. The highly pure N_2 was used in the sorption experiments, the gases isotherms was measured at 77 K. Water adsorption experiment was performed by volumetric method using a IGA100B instrument at 25 °C.

2.4. Proton conductivity measurements

Typically, the H_2SO_4@$(NH_2)_x$-MIL-125 (x = 0, 1 or 2) powders were evaluated from electrochemical impedance spectroscopy for the compressed pellets of the powdered samples at controlled humidity and temperatures. The pellets of bulk samples (H_2SO_4@MIL-125: 2.5 mm in diameter and 0.63 mm in thickness; H_2SO_4@NH_2-MIL-125: 2.5 mm in diameter and 0.72 mm in thickness; H_2SO_4@$(NH_2)_2$-MIL-125: 2.5 mm in diameter and 0.73 mm in thickness) were compressed under a pressure of ~500 Mpa to ensure good contact, then both sides of the pellet were attached to gold wires (50 μm) with silver paste. AC electrochemical impedance measurements were performed by the conventional quasi-four-probe method with a Solartron SI 1260 Impedance/Gain-Phase Analyzer. The device impedance was measured by applying 200 mV ac voltage whose frequency (ω) is swept from 1 to 1 × 10^7 Hz in 10 steps on a logarithmic scale under controlled humidity and temperature environments. Exposure of the samples to controlled humidity and temperature environments was performed using an XK-CTS80Z (Shenzhen selenium control testing equipment corp.) humidity control oven. Experiments were performed in air, at temperatures between 40 and 80 °C while humidity levels were maintained at 98% relative humidity (RH). The impedance spectra were analyzed with ZView2 (Scribner Associates), a software which was used to generate Nyquist plots and fit the data. The proton conductivity (σ, S.cm^{-1}) was estimated by using the equation:

$$\sigma = L/RS \tag{1}$$

where, L is the thickness, S is the area of the measured plate; R (Ω) is the measured resistance from the Nyquist plot. The activation energy (E_a) is calculated by using the conductivity data between 40 and 80 °C at 98% RH with the Arrhenius equation:

$$\ln(\sigma T) = \ln A - E_a/(k_B T) \tag{2}$$

where k_B and A are the Boltzmann constant and the pre-exponential factor, respectively.

3. Results and discussion

As show in Fig. 1, $(NH_2)_x$-MIL-125 (x = 0, 1 or 2) were directly synthesized as a crystalline powder through one-pot solvothermal method. In brief, benzenedicarboxylate-$(NH_2)_x$ and titanium *n*-butoxide were taken into a solvent mixture of dry N, N-dimethylformamide (DMF) and methanol (MeOH). The $(NH_2)_x$-MIL-125 (x = 0, 1 or 2) immersed in 1 M H_2SO_4 aqueous solution and then thoroughly washed with MeOH, then dried to give the pure phase of the H_2SO_4@$(NH_2)_x$-MIL-125 (x = 0, 1 or 2) (details see Supporting Information, SI).

The morphology and purity of $(NH_2)_x$-MIL-125(x = 0, 1 or 2) and H_2SO_4@$(NH_2)_x$-MIL-125(x = 0, 1 or 2) were confirmed by transmission electron microscopy (TEM) and scanning electron microscopy (SEM) (Fig. 2 and Fig. S1), showing a homogeneous nanosheet-like morphologies. After H_2SO_4 treatment, the resulted H_2SO_4@$(NH_2)_x$-MIL-125 (x = 0, 1 or 2) materials became thinner and smaller when compared with the corresponding $(NH_2)_x$-MIL-125 (x = 0, 1 or 2).

Powder X-ray diffraction (PXRD) analysis of $(NH_2)_x$-MIL-125 (x = 0, 1 or 2) before and after H_2SO_4 treatment indicates its structural stability towards acid treatment (Fig. 3a and S2). As shown in Fig. 3b and S3-4, from the instantaneous color change of MOFs after acid treatment, we found that the H_2SO_4treatment process of $(NH_2)_x$-MIL-125 (x = 0, 1 or 2) was fast and irreversible with the color changed from yellow to brown for NH_2-MIL-125, and from dark brown to red brown for $(NH_2)_2$-MIL-125. It is worth noting that for the MIL-125, i.e., without amine functional groups, no significant color change was observed, clearly suggesting that the indispensable of amino groups of MOF and H_2SO_4 strong interactions build from Brønsted acid–base pairs formation[2]. In the fourier transform infrared (FT-IR) spectra (Fig. 3c), a peak at 1068 $cm^{-1}$of H_2SO_4@$(NH_2)_2$-MIL-125 corresponds to the symmetric vibration of $-SO_3^-$ and which is absent for $(NH_2)_2$-MIL-125 [2,4,47]. The peaks between about 2800 and 3700 cm^{-1} can be ascribed to amino groups [47]. Thermo-gravimetric analysis (TGA) of the H_2SO_4@$(NH_2)_2$-MIL-125 under N_2 atmosphere revealed that the release

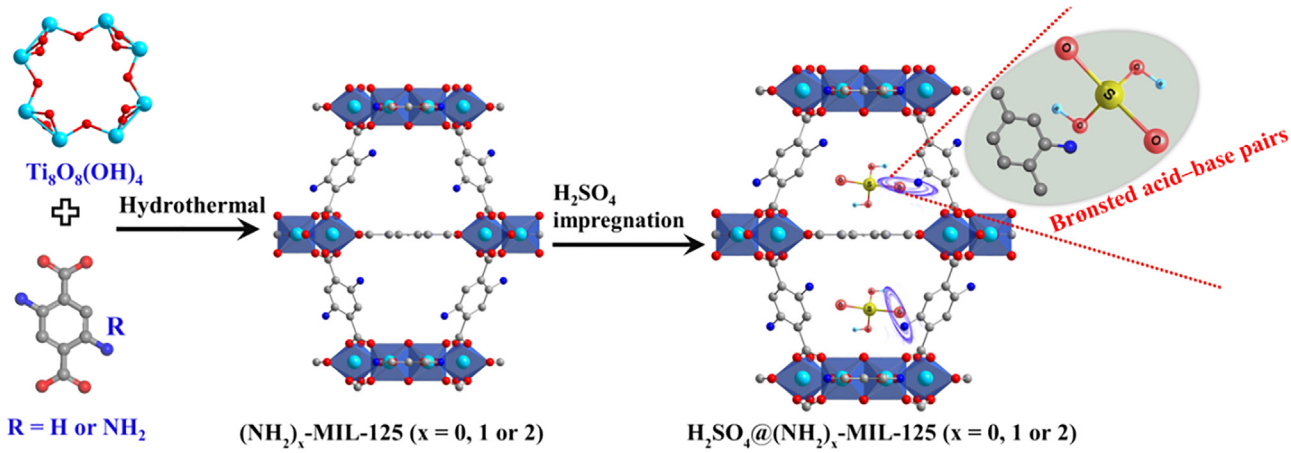

Fig. 1. Schematic of the preparation of $H_2SO_4@(NH_2)_x$ -MIL-125 (x = 0, 1 or 2), carbon, gray; oxygen, red; nitrogen, mazarine; titanium, azure. (For interpretation of the references to color in this figure legend, the reader is referred to the web version of this article.)

of water molecules or attached solvent when the temperature is above 100 °C, the irreversible decompose of the MOF took place at above 330–350 °C (Fig. 3d). The N_2-physisorption measurements at 77 K revealed that the isotherm curves are a combination of type I and type II, which are the typical permanent microporosity. Surface area of $(NH_2)_2$-MIL-125 and $H_2SO_4@(NH_2)_2$-MIL-125, obtained from the Brunauer–-Emmett–Teller (BET), are 1030 ± 20 and 360 ± 20 m^2/g, respectively (Fig. 3e). The decreased surface area after acid treatment for MOF reflects the reduced pore volume upon $-SO_3H$ moities insertion·H_2O plays a key role, generates H-bond networks in the H_2O-assisted proton conductors. So to confirm the wetability of the pores of $H_2SO_4@(NH_2)_2$-MIL-125, the water vapor adsorption was performed at 25 °C (Fig. 3f), the adsorption amounts of H_2O increases as the vapor pressure get increased, up to 30% mass at $P/P_0 = 1$. The water sorption isotherms exhibited obvious hysteresis behavior, meaning that the H_2O are absorbed into the micropores of $H_2SO_4@(NH_2)_2$-MIL-125.

All the above results show that the good stability, strong Brønsted acid-base interaction and good wettability, enable $H_2SO_4@(NH_2)_2$-MIL-125 as a potential candidate for proton-conducting materials.

3.1. Proton conductivity

The proton conductivity (σ, S cm^{-1}) of $H_2SO_4@(NH_2)_x$-MIL-125 (x = 0, 1 or 2) pelletized samples were carried out by alternating-current (a.c.) impedance at controlled environment (Fig. 4a, 4c and S5). The Nyquist plots obtained were consisted of a single semicircle or arcs at high-frequency and a capacitive tail at low frequency regions. In detail, semicircle is representative of bulk and grain boundary resistance and the tailis corresponding to ionic conductivity blocked by the silver electrodes [2,34,37], the conductivity was calculated from the Eq. (1).

Humidity-dependent conductivity of $H_2SO_4@(NH_2)_x$-MIL-125 (x = 0, 1 or 2) were measured by maintain the sample at a constant temperature of 80 °C (Fig. 4a, 4b and S5). For H_2SO_4@MIL-125, $H_2SO_4@NH_2$-MIL-125 and $H_2SO_4@(NH_2)_2$-MIL-125, low conductivity of 1.5×10^{-8}, 1.5×10^{-7}, 6.7×10^{-7} S cm^{-1} at 40% RH were obtained, respectively. The σ dramatically increased to 4.9×10^{-6}, 6.4×10^{-5}, 4.9×10^{-4} S cm^{-1} at 90% RH, respectively. When the measurements conditions were set to 98% RH, the σ of H_2SO_4@MIL-125, $H_2SO_4@NH_2$-MIL-125 and $H_2SO_4@(NH_2)_2$-MIL-125 increased to 6.3×10^{-5}, 4.9×10^{-4}, 2.2×10^{-2} S cm^{-1}, respectively. It's worth

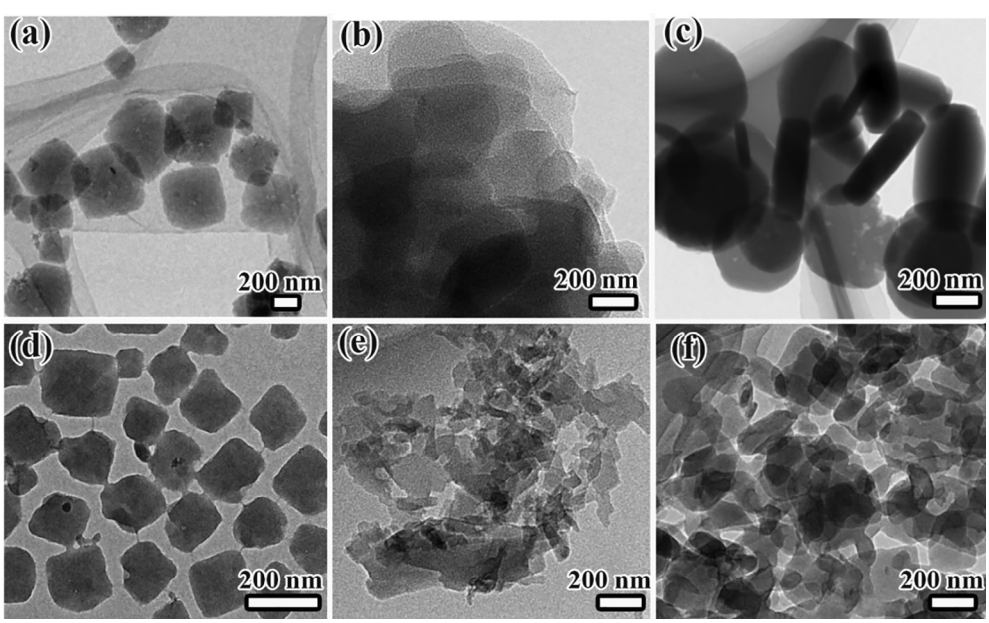

Fig. 2. TEM images of (a) MIL-125, (b) NH_2-MIL-125, (c) $(NH_2)_2$-MIL-125, (d) H_2SO_4@MIL-125, (e) $H_2SO_4@NH_2$-MIL-125, (f) $H_2SO_4@(NH_2)_2$-MIL-125, respectively.

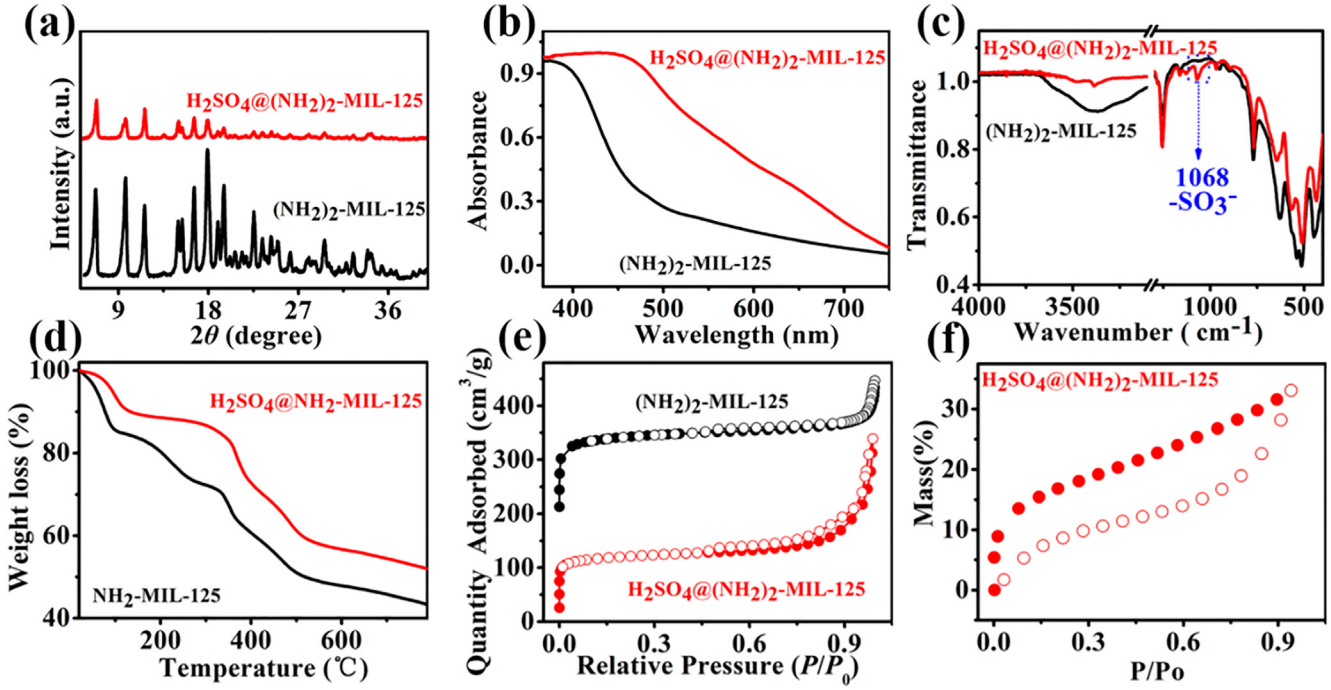

Fig. 3. (a)The PXRD patterns of $(NH_2)_2$-MIL-125 and H_2SO_4@$(NH_2)_2$-MIL-125, (b)UV–vis absorption spectrums of $(NH_2)_2$-MIL-125 and H_2SO_4@$(NH_2)_2$-MIL-125, (c) FT-IR stretching patterns of $(NH_2)_2$-MIL-125 and H_2SO_4@$(NH_2)_2$-MIL-125, the peak at 1068 cm^{-1} of the H_2SO_4@$(NH_2)_2$-MIL-125 spectra can be assigned to the symmetric vibration of $–SO_3^-$, (d)TGA curve of $(NH_2)_2$-MIL-125 and H_2SO_4@$(NH_2)_2$-MIL-125, (e)Nitrogen sorption isotherms for $(NH_2)_2$-MIL-125 and H_2SO_4@$(NH_2)_2$-MIL-125(f)Adsorption-desorption experiments of water vapor on H_2SO_4@$(NH_2)_2$-MIL-125 at 25 °C.

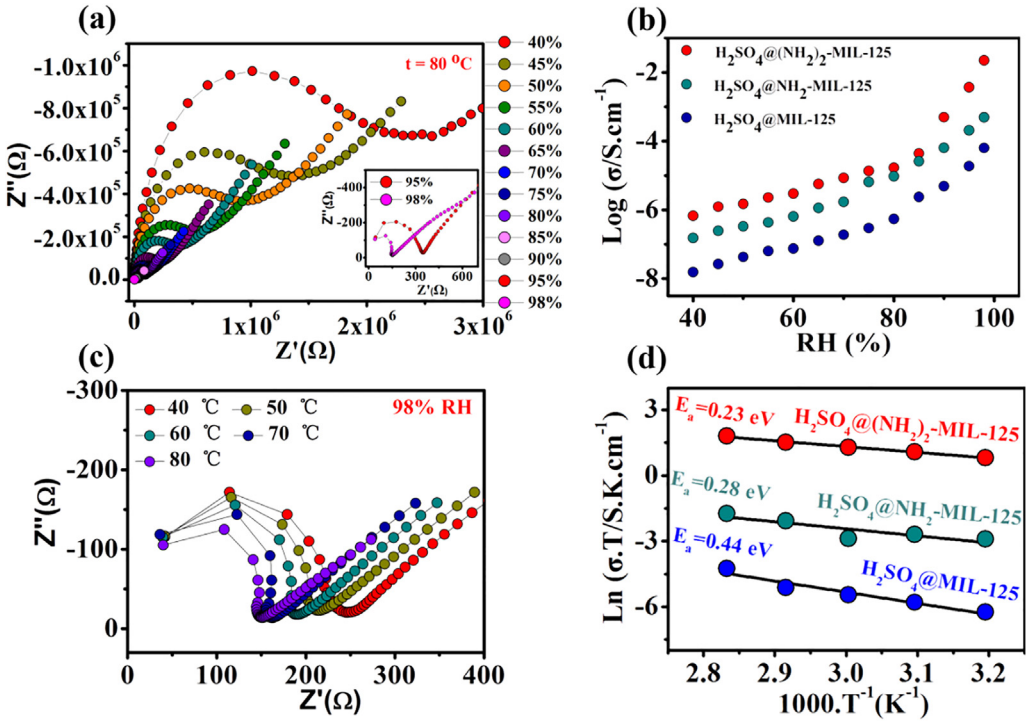

Fig. 4. Proton conductivity of H_2SO_4@$(NH_2)_x$-MIL-125 (x = 0, 1 and 2). (a) RH-dependent impedance plots of H_2SO_4@$(NH_2)_2$-MIL-125 at 80 °C, (inset) Typical Nyquist plots of the H_2SO_4@$(NH_2)_2$-MIL-125 at 80 °C&95% RH and at 80 °C&98% RH .(b) Log-scaled σ of H_2SO_4@$(NH_2)_x$-MIL-125 (x = 0, 1 and 2) at various RHs.(c) Temperature-dependent impedance plots of H_2SO_4@$(NH_2)_2$-MIL-125 at 98% RH. (d) Arrhenius plots of H_2SO_4@$(NH_2)_x$-MIL-125 (x = 0, 1 and 2).

mentioning that the σ of 2.2×10^{-2} S cm^{-1} of H_2SO_4@$(NH_2)_2$-MIL-125 can be compared with the highest σ of MOFs/CPs proton conductor (Table 1 in SI). The proton conductivities of H_2SO_4@$(NH_2)_2$-MIL-125 increase with the RH, it is quasi-linearly in the low RH range of 40 ~ 80%, but rapidly increased after above 80% RH. The trend is in line with the water vapor adsorption isotherm, that is means the proton primarily migrationrelies heavily on the water content and through the MOFs pores [41].

The temperature-dependent proton conductivities were further examined at 98% RH. Fig. 4c and Fig. S5b and d show the Nyquist plots of the proton conductivity. The σ for H_2SO_4@MIL-125, H_2SO_4@NH_2-MIL-125 and H_2SO_4@$(NH_2)_2$-MIL-125 were calculated to be 6.2×10^{-6}, 1.7×10^{-4}, 7.2×10^{-3} S cm^{-1}, respectively, at 40 °C &98% RH. The σ value increases with temperature and were 6.3×10^{-5}, 4.9×10^{-4}, 2.2×10^{-2} S cm^{-1} at 80 °C, respectively. The activation energy (E_a) is calculated by fitting the σ data with the Arrhenius equation (Please

check the Eq. (2)). H_2SO_4@MIL-125, H_2SO_4@NH_2-MIL-125 and H_2SO_4@$(NH_2)_2$-MIL-125 demonstrated Arrhenius behavior with an E_a of 0.44, 0.28 and 0.23 eV, respectively (Fig. 4d). E_a (0.23 eV) of H_2SO_4@$(NH_2)_2$-MIL-125 is quite small and consistent with Nafion (E_a = 0.22 eV), a typical hydrated proton conductors [48]. The high σ and low E_a at high humidity may due to the almost completely dominated of the intra-channel H_2O sites, confirming a fast ion conducting behavior between adjacent $(NH_2)^+\cdots HSO_4^-\cdots H_3O^+$ triads, as rationalized based on the Grotthuss-type hopping mechanism [1,49–50]. But the alternative vehicular mechanism of H_2SO_4@MIL-125 is associated with E_a values above 0.4 eV [41]. Temperature-dependent impedance plots of H_2SO_4@$(NH_2)_2$-MIL-125 were reproducible during heating and cooling cycles under 98% RH, indicating good recyclability up to 4 runs (Fig. S6). PXRD analysis further confirmed that the framework of H_2SO_4@$(NH_2)_2$-MIL-125 maintained its structural integrity after proton conductivity measurements (Fig. S7).

Another interesting result is that the σ gradual increased with the increasing the amino functional group of H_2SO_4@$(NH_2)_x$-MIL-125 (x = 0, 1 or 2). The σ value of H_2SO_4@$(NH_2)_2$-MIL-125 under the same conditions is much higher than those of H_2SO_4@MIL-125 and H_2SO_4@NH_2-MIL-125. Taking into account the change of the color of the $(NH_2)_x$-MIL-125 (x = 1 or 2) after H_2SO_4 treatment, sulfonic acid groups (Brønsted acid sites)[1] might have formed Brønsted acid–base pairs with the existence of $-NH_2$ group (Brønsted base sites) on the organic linkers [2]. We proposed that the included dangling sulfonic acid groups will increased as amino groups increase. Finally, acid–base pair unitsplay a key role for the high proton conductivity [2].

4. Conclusions

In summary, a high proton conductive complex, H_2SO_4@$(NH_2)_2$-MIL-125, was synthesized by a facile impregnation way. The unique Brønsted acid–base pairs formed between H_2SO_4 and amino group of MOF build high-density H-bonding networks. Our results demonstrated that the increased proton conductivity with the increased amino functional group of H_2SO_4@$(NH_2)_x$-MIL-125 (x = 0, 1 or 2). The proton conductivity value of H_2SO_4@$(NH_2)_2$-MIL-125 reaches to 2.2×10^{-2} at 80 °C & 98%RH, and can be compared to those of the best proton conduits of MOFs and Nafion. The high proton conductivity of H_2SO_4@$(NH_2)_2$-MIL-125 under high humidity atmospheres can be attributed to the Brønstedacid–base pair units. The results could provide a simple yet effective way to optimize the proton conducting properties of MOFs.

Declaration of competing interest

The authors declare no competing financial interest.

Acknowledgments

This work was supported by Key Research Program of Frontier Science, CAS (QYZDB-SSW-SLH023), NSFC (21805276, 21773245, 21822109, 21801243, 51602311, 21850410462), Project Funded by China Postdoctoral Science Fundation (2018M642576, 2018M642578) and NSF of Fujian Province (2017J05094, 2019J01129), International Partnership Program of CAS (121835KYSB201800).

Appendix A. Supplementary data

Supplementary data to this article can be found online at https://doi.org/10.1016/j.ica.2019.119317.

References

[1] W.J. Phang, H. Jo, W.R. Lee, J.H. Song, K. Yoo, B. Kim, C.S. Hong, Superprotonic conductivity of a UiO-66 framework functionalized with sulfonic acid groups by facile postsynthetic oxidation, Angew. Chem. Int. Ed. 54 (2015) 5142.
[2] S.S. Nagarkar, S.M. Unni, A. Sharma, S. Kurungot, S.K. Ghosh, Two-in-one: inherent anhydrous and water-assisted high proton conduction in a 3D metal-organic framework, Angew. Chem. Int. Ed. 53 (2014) 2638.
[3] M. Yoon, K. Suh, S. Natarajan, K. Kim, Proton conduction in metal-organic frameworks and related modularly built porous solids, Angew. Chem. Int. Ed. 52 (2013) 2688.
[4] F. Yang, G. Xu, Y. Dou, B. Wang, H. Zhang, H. Wu, W. Zhou, J.-R. Li, B. Chen, A flexible metal-organic framework with a high density of sulfonic acid sites for proton conduction, Nature Energy 2 (2017).
[5] H. Xu, S. Tao, D. Jiang, Proton conduction in crystalline and porous covalent organic frameworks, Nature Mater. 15 (2016) 722.
[6] J.M. Taylor, K.W. Dawson, G.K.H. Shimizu, A water-stable metal-organic framework with highly acidic pores for proton-conducting applications, J. Am. Chem. Soc. 135 (2013) 1193.
[7] G.B. Gardner, D. Venkataraman, J.S. Moore, S. Lee, Spontaneous assembly of a hinged coordination network, Nature 374 (1995) 792.
[8] H.K. Chae, D.Y. Siberio-Perez, J. Kim, Y. Go, M. Eddaoudi, A.J. Matzger, M. O'Keeffe, O.M. Yaghi, A route to high surface area, porosity and inclusion of large molecules in crystals, Nature 427 (2004) 523.
[9] S. Shimomura, M. Higuchi, R. Matsuda, K. Yoneda, Y. Hijikata, Y. Kubota, Y. Mita, J. Kim, M. Takata, S. Kitagawa, Selective sorption of oxygen and nitric oxide by an electron-donating flexible porous coordination polymer, Nature Chem. 2 (2010) 633.
[10] G. Ferey, C. Mellot-Draznieks, C. Serre, F. Millange, J. Dutour, S. Surble, I. Margiolaki, A chromium terephthalate-based solid with unusually large pore volumes and surface area, Science 309 (2005) 2040.
[11] K. Shen, L. Zhang, X. Chen, L. Liu, D. Zhang, Y. Han, J. Chen, J. Long, R. Luque, Y. Li, B. Chen, Ordered macro-microporous metal-organic framework single crystals, Science 359 (2018) 206.
[12] S.S. Nagarkar, B. Joarder, A.K. Chaudhari, S. Mukherjee, S.K. Ghosh, Highly selective detection of nitro explosives by a luminescent metal-organic framework, Angew. Chem. Int. Ed. 52 (2013) 2881.
[13] M.B. Chambers, X. Wang, L. Ellezam, O. Ersen, M. Fontecave, C. Sanchez, L. Rozes, C. Mellot-Draznieks, Maximizing the photocatalytic activity of metal-organic frameworks with aminated-functionalized linkers: substoichiometric effects in MIL-125-NH2, J. Am. Chem. Soc. 139 (2017) 8222.
[14] T. Zhang, W. Lin, Metal-organic frameworks for artificial photosynthesis and photocatalysis, Chem. Soc. Rev. 43 (2014) 5982.
[15] P.-Q. Liao, N.-Y. Huang, W.-X. Zhang, J.-P. Zhang, X.-M. Chen, Controlling guest conformation for efficient purification of butadiene, Science. 356 (2017) 1193.
[16] L. Chen, J.-W. Ye, H.-P. Wang, M. Pan, S.-Y. Yin, Z.-W. Wei, L.-Y. Zhang, K. Wu, Y.-N. Fan, C.-Y. Su, Ultrafast water sensing and thermal imaging by a metal-organic framework with switchable luminescence, Nat. Commun. 8 (2017).
[17] F. Moreau, I. da Silva, N.H. Al Smail, T.L. Easun, M. Savage, H.G.W. Godfrey, S.F. Parker, P. Manuel, S. Yang, M. Schroeder, Unravelling exceptional acetylene and carbon dioxide adsorption within a tetra-amide functionalized metal-organic framework, Nat. Commun. 8 (2017).
[18] S. Sakaida, K. Otsubo, O. Sakata, C. Song, A. Fujiwara, M. Takata, H. Kitagawa, Crystalline coordination framework endowed with dynamic gate-opening behaviour by being downsized to a thin film, Nature Chem. 8 (2016) 377.
[19] M. Ding, R.W. Flaig, H.-L. Jiang, O.M. Yaghi, Carbon capture and conversion using metal-organic frameworks and MOF-based materials, Chem. Soc. Rev. 48 (2019) 2783.
[20] Y. Zheng, H. Sato, P. Wu, H.J. Jeon, R. Matsuda, S. Kitagawa, Flexible interlocked porous frameworks allow quantitative photoisomerization in a crystalline solid, Nat. Commun. (2017,8.).
[21] R.-B. Lin, L. Li, H.-L. Zhou, H. Wu, C. He, S. Li, R. Krishna, J. Li, W. Zhou, B. Chen, Molecular sieving of ethylene from ethane using a rigid metal-organic framework, Nature Mater. 17 (2018) 1128.
[22] C.A. Trickett, T.M.O. Popp, J. Su, C. Yan, J. Weisberg, A. Huq, P. Urban, J. Jiang, M.J. Kalmutzki, Q. Liu, J. Baek, M.P. Head-Gordon, G.A. Somorjai, J.A. Reimer, O.M. Yaghi, Identification of the strong Bronsted acid site in a metal-organic framework solid acid catalyst, Nature Chem. 11 (2019) 170.
[23] F.-M. Zhang, L.-Z. Dong, J.-S. Qin, W. Guan, J. Liu, S.-L. Li, M. Lu, Y.-Q. Lan, Z.-M. Su, H.-C. Zhou, Effect of imidazole arrangements on proton-conductivity in metal-organic frameworks, J. Am. Chem. Soc. 139 (2017) 6183.
[24] T. Haraguchi, K. Otsubo, O. Sokota, A. Fujiwara, H. Kitagawa, Guest-induced two-way structural transformation in a layered metal-organic framework thin film, J. Am. Chem. Soc. 138 (2016) 16787.
[25] A. Kirchon, L. Feng, H.F. Drake, E.A. Joseph, H.-C. Zhou, From fundamentals to applications: a toolbox for robust and multifunctional MOF materials, Chem. Soc. Rev. 47 (2018) 8611.
[26] N. Tsumori, L. Chen, Q. Wang, Q.-L. Zhu, M. Kitta, Q. Xu, Quasi-MOF: exposing inorganic nodes to guest metal nanoparticles for drastically enhanced catalytic activity, Chem 4 (2018) 845.
[27] Z. Liang, C. Qu, D. Xia, R. Zou, Q. Xu, Atomically dispersed metal sites in MOF-based materials for electrocatalytic and photocatalytic energy conversion, Angew. Chem. Int. Ed. 57 (2018) 9604.
[28] H. He, Y. Cui, B. Li, B. Wang, C. Jin, J. Yu, L. Yao, Y. Yang, B. Chen, G. Qian, Confinement of perovskite-QDs within a single MOF crystal for significantly enhanced multiphoton excited luminescence, Adv. Mater. 31 (2019).
[29] R.-W. Huang, Y.-S. Wei, X.-Y. Dong, X.-H. Wu, C.-X. Du, S.-Q. Zang, T.C.W. Mak, Hypersensitive dual-function luminescence switching of a silver-chalcogenolate cluster-based metal-organic framework, Nature Chem. 9 (2017) 689.
[30] F.-M. Zhang, J.-L. Sheng, Z.-D. Yang, X.-J. Sun, H.-L. Tang, M. Lu, H. Dong, F.-

C. Shen, J. Liu, Y.-Q. Lan, Rational design of MOF/COF hybrid materials for photocatalytic H-2 evolution in the presence of sacrificial electron donors, Angew. Chem. Int. Ed. 57 (2018) 12106.
[31] W.-T. Koo, J.-S. Jang, I.-D. Kim, Metal-organic frameworks for chemiresistive sensors, Chem (2019).
[32] H. Furukawa, K.E. Cordova, M. O'Keeffe, O.M. Yaghi, The chemistry and applications of metal-organic frameworks, Science 341 (2013) 974.
[33] G.K.H. Shimizu, J.M. Taylor, S. Kim, Proton conduction with metal-organic frameworks, Science 341 (2013) 354.
[34] N.E. Wong, P. Ramaswamy, A.S. Lee, B.S. Gelfand, K.J. Bladek, J.M. Taylor, D.M. Spasyuk, G.K.H. Shimizu, Tuning intrinsic and extrinsic proton conduction in metal-organic frameworks by the lanthanide contraction, J. Am. Chem. Soc. 139 (2017) 14676.
[35] S. Kim, B. Joarder, J.A. Hurd, J. Zhang, K.W. Dawson, B.S. Gelfand, N.E. Wong, G.K.H. Shimizu, Achieving superprotonic conduction in metal-organic frameworks through iterative design advances, J. Am. Chem. Soc. 140 (2018) 1077.
[36] G. Xu, K. Otsubo, T. Yamada, S. Sakaida, H. Kitagawa, Superprotonic conductivity in a highly oriented crystalline metal-organic framework nanofilm, J. Am. Chem. Soc. 135 (2013) 7438.
[37] J.A. Hurd, R. Vaidhyanathan, V. Thangadurai, C.I. Ratcliffe, I.L. Moudrakovski, G.K.H. Shimizu, Anhydrous proton conduction at 150 degrees C in a crystalline metal-organic framework, Nature Chem. 1 (2009) 705.
[38] M. Sadakiyo, T. Yamada, K. Honda, H. Matsui, H. Kitagawa, Control of crystalline proton-conducting pathways by water-induced transformations of hydrogen-bonding networks in a metal-organic framework, J. Am. Chem. Soc. 136 (2014) 7701.
[39] T. Yamada, K. Otsubo, R. Makiura, H. Kitagawa, Designer coordination polymers: dimensional crossover architectures and proton conduction, Chem. Soc. Rev. 42 (2013) 6655.
[40] X. Meng, H.-N. Wang, S.-Y. Song, H.-J. Zhang, Proton-conducting crystalline porous materials, Chem. Soc. Rev. 46 (2017) 464.
[41] V.G. Ponomareva, K.A. Kovalenko, A.P. Chupakhin, D.N. Dybtsev, E.S. Shutova, V.P. Fedin, Imparting high proton conductivity to a metal-organic framework material by controlled acid impregnation, J. Am. Chem. Soc. 134 (2012) 15640.
[42] M. Sadakiyo, T. Yamada, H. Kitagawa, Rational designs for highly proton-conductive metal-organic frameworks, J. Am. Chem. Soc. 131 (2009) 9906.
[43] M.G. Goesten, J. Juan-Alcaniz, E.V. Ramos-Fernandez, K.B.S.S. Gupta, E. Stavitski, H. van Bekkum, J. Gascon, F. Kapteijn, Sulfation of metal-organic frameworks: Opportunities for acid catalysis and proton conductivity, J. Catal. 281 (2011) 177.
[44] X.-L. Sun, W.-H. Deng, H. Chen, H.-L. Han, J.M. Taylor, C.-Q. Wan, G. Xu, A metal-organic framework impregnated with a binary ionic liquid for safe proton conduction above 100 degrees C, Chem. Eur. J. 23 (2017) 1248.
[45] D. Gui, X. Dai, Z. Tao, T. Zheng, X. Wang, M.A. Silver, J. Shu, L. Chen, Y. Wang, T. Zhang, J. Xie, L. Zou, Y. Xia, J. Zhang, J. Zhang, L. Zhao, J. Diwu, R. Zhou, Z. Chai, S. Wang, Unique proton transportation pathway in a robust inorganic coordination polymer leading to intrinsically high and sustainable anhydrous proton conductivity, J. Am. Chem. Soc. 140 (2018) 6146.
[46] C.H. Hendon, D. Tiana, M. Fontecave, C. Sanchez, L. D'Arras, C. Sassoye, L. Rozes, C. Mellot-Draznieks, A. Walsh, Engineering the optical response of the titanium-MIL-125 metal-organic framework through ligand functionalization, J. Am. Chem. Soc. 135 (2013) 10942.
[47] C.-R. Li, S.-L. Li, X.-M. Zhang, D-3-symmetric supramolecular cation $\{(Me_2NH_2)(6)(SO_4)\}(4+)$ as a new template for 3D homochiral (10,3)-a metal oxalates, Cryst. Growth Des. 9 (2009) 1702.
[48] X. Wu, X. Wang, G. He, J. Benziger, Differences in water sorption and proton conductivity between nafion and SPEEK, J. Polym. Sci., Part B: Polym. 49 (2011) 1437.
[49] P. Ramaswamy, N.E. Wong, G.K.H. Shimizu, MOFs as proton conductors - challenges and opportunities, Chem. Soc. Rev. 43 (2014) 5913.
[50] N.F. Zheng, X.H. Bu, P.Y. Feng, Synthetic design of crystalline inorganic chalcogenides exhibiting fast-ion conductivity, Nature. 426 (2003) 428.